SLAC–PUB–11344
July 2005

Determination of Littlest Higgs Model Parameters at the ILC* †

John A. Conley[a], JoAnne Hewett[b], and My Phuong Le[c]
Stanford Linear Accelerator Center, Stanford University, Stanford, CA 94309

Abstract

We examine the effects of the extended gauge sector of the Littlest Higgs model in high energy e^+e^- collisions. We find that the search reach in $e^+e^- \to f\bar{f}$ at a $\sqrt{s} = 500\,\mathrm{GeV}$ International Linear Collider covers essentially the entire parameter region where the Littlest Higgs model is relevant to the gauge hierarchy problem. In addition, we show that this channel provides an accurate determination of the fundamental model parameters, to the precision of a few percent, provided that the LHC measures the mass of the heavy neutral gauge field. Additionally, we show that the couplings of the extra gauge bosons to the light Higgs can be observed from the process $e^+e^- \to Zh$ for a significant region of the parameter space. This allows for confirmation of the structure of the cancelation of the Higgs mass quadratic divergence and would verify the little Higgs mechanism.

Submitted to Physical Review D

*Work supported by Department of Energy contract DE-AC02-76SF00515.
†e-mails: [a]conley@stanford.edu, [b]hewett@slac.stanford.edu, and [c]myphle@stanford.edu

1 Introduction

The Standard Model (SM) of particle physics is a remarkably successful theory. It provides a complete description of physics at currently accessible energies, and its predictions have been confirmed to high accuracy by all high energy experiments to date. An important piece of the SM remains unexplained–the mechanism of electroweak symmetry breaking. Precision measurements and direct searches suggest that this mechanism involves a weakly coupled Higgs boson with a mass in the range $114 < m_H < 208\,\mathrm{GeV}$ at 95% CL. The Higgs mass parameter, however, is quadratically sensitive to UV physics. New physics at the TeV scale is therefore necessary to keep the Higgs light without fine-tuning. This is known as the hierarchy problem. Three main classes of models, supersymmetry, extra dimensions, and little Higgs, have been proposed to address the hierarchy problem. Which of these theories Nature has chosen will be determined in the coming years as the Large Hadron Collider and the International Linear Collider probe the TeV scale.

The little Higgs models [1, 2, 3] feature the Higgs as a pseudo Nambu-Goldstone boson of an approximate global symmetry which is broken by a vev at a scale of a few TeV. The breaking is realized in such a way that the Higgs mass only receives quantum corrections at two loops. In contrast to supersymmetry, the one-loop contribution to the Higgs mass from a SM particle is canceled by a contribution from a new particle of the *same* spin. Little Higgs theories thus predict the existence of new top-like quarks, gauge bosons, and scalars near the TeV scale. The distinguishing features of this model are the existence of these new particles and their couplings to the light Higgs. Measurement of these couplings would verify the structure of the cancelation of the Higgs mass quadratic divergences and prove the existence of the little Higgs mechanism.

The most economical little Higgs model is the so-called "Littlest Higgs" (LH) [1], which we introduce here and describe in more detail in Sec. 2. This scenario is based on a non-linear sigma model with an $SU(5)$ global symmetry, which is broken to the subgroup $SO(5)$ by a vev f. The vev is generated by some strongly coupled physics at a scale $\Lambda_S \sim 4\pi f$; possible UV completions of little Higgs theories are discussed in [3, 4]. The $SU(5)$ contains a gauged subgroup $[SU(2) \times U(1)]^2$ which is broken by the vev to the SM electroweak group $[SU(2)_L \times U(1)_Y]$. The global $SU(5)$ breaking leaves 14 massless Goldstone bosons, four of which are eaten by the gauge bosons of the broken gauge groups, giving these gauge bosons a mass of order f. In particular, we have a heavy Z-like boson Z_H and a heavy photon-like boson A_H which, as we will see, are phenomenologically important. The other ten Goldstone bosons make up a complex doublet and a complex triplet which remain massless at this stage. Masses for the complex triplet are generated at the TeV-scale by one-loop gauge interactions. The neutral component of the complex doublet plays the role of the SM Higgs. Its mass term comes from a Coleman-Weinberg potential and has quadratically divergent corrections only at two loops, giving $\mu^2 \sim f^2/16\pi^2$. Thus the natural scale for f is around a TeV. If f is much higher than a few TeV, the Higgs mass must again be finely tuned and this model no longer addresses the hierarchy problem.

The phenomenological implications of little Higgs models have been explored in [1, 5, 6, 7, 8, 9, 10, 11]. Constraints arise from electroweak precision data as well as from indirect and

direct production at LEP-II and the Tevatron. For example, in the Littlest Higgs scenario, the lack of discovery of the A_H, which is expected to be quite light, puts a lower bound on f in the few TeV range. Significant electroweak constraints come from tree-level and loop deviations of the ρ-parameter and the weak mixing angle $\sin^2\theta_w$ from their SM values. Combining these gives a limit $f \gtrsim 4\,\mathrm{TeV}$ which is relatively parameter independent. Many variants of little Higgs models exist in the literature which lower this bound to $f \gtrsim 1-2\,\mathrm{TeV}$.

In this paper we use the processes $e^+e^- \to f\bar{f}$ and $e^+e^- \to Zh$ to investigate experimental limits from LEP II data on the Littlest Higgs parameters, to evaluate the extent of the International Linear Collider's search reach in LH parameter space, and to see how accurately the ILC will be able to determine the LH parameters. Complementary discussions of the Littlest Higgs model at the ILC and LHC can be found in [10, 11]. In Sec. 2, we discuss the Littlest Higgs model in detail. In Sec. 3, we examine the process $e^+e^- \to f\bar{f}$ at LEP II and the ILC and determine how accurately the ILC will be able to measure the LH parameters. In Sec. 4 we explore the LH parameter space using the process $e^+e^- \to Zh$ at the ILC.

2 The Littlest Higgs model and its parameters

In this paper, we are mainly concerned with the extended neutral gauge sector present in the LH model. While this scenario also includes a number of parameters that arise from the top and scalar sectors, in which there are a number of new heavy particles, the observables of concern in our analysis only depend on the three parameters present in the extended heavy gauge sector. These are f, the vev or "pion decay constant" of the nonlinear sigma model, which we discussed in the Introduction, and two mixing angles. Although we focus on the Littlest Higgs model, we note that an enlarged gauge sector with rather generic features is present in all little Higgs scenarios.

The vev f characterizes the scale of the $SU(5) \to SO(5)$ breaking; the effective field theory of the 14 Goldstone bosons has the Lagrangian

$$\mathcal{L}_\Sigma = \frac{1}{2}\frac{f^2}{4}\mathrm{Tr}\,|\mathcal{D}_\mu\Sigma|^2\,, \tag{1}$$

where Σ is a 5×5 matrix parametrization of the Goldstone boson degrees of freedom [1, 11]. The covariant derivative contains the gauge bosons associated with the gauged subgroup $[SU(2)\times U(1)]^2$, W_1, W_2, B_1, and B_2;

$$\mathcal{D}_\mu\Sigma = \partial_\mu\Sigma - i\sum_{j=1}^{2}\left(g_j(W_j\Sigma + \Sigma W_j^T) + g_j'(B_j\Sigma + \Sigma B_j^T)\right). \tag{2}$$

At the same time, the $[SU(2)\times U(1)]^2$ is also broken to $[SU(2)_L\times U(1)_Y]$, and the gauge boson mass eigenstates after the symmetry breaking are

$$\begin{aligned} W &= sW_1 + cW_2, \quad W' = -cW_1 + sW_2, \\ B &= s'B_1 + c'B_2, \quad B' = -c'B_1 + s'B_2. \end{aligned} \tag{3}$$

The W are the massless gauge bosons associated with the generators of $SU(2)_L$ and the B is the massless gauge boson associated with the generator of $U(1)_Y$. The W' and B' are the massive gauge bosons associated with the four broken generators of $[SU(2) \times U(1)]^2$, with their masses being given by

$$m_{W'} = \frac{f}{2}\sqrt{g_1^2 + g_2^2} = \frac{g}{2sc}f, \quad m_{B'} = \frac{f}{2\sqrt{5}}\sqrt{g_1'^2 + g_2'^2} = \frac{g}{2\sqrt{5}s'c'}f. \tag{4}$$

The mixing angles

$$s = \frac{g_2}{\sqrt{g_1^2 + g_2^2}} \text{ and } s' = \frac{g_2'}{\sqrt{g_1'^2 + g_2'^2}} \tag{5}$$

relate the coupling strengths of the two copies of $[SU(2) \times U(1)]$. These two angles together with f are the three parameters of the model that are relevant to our analysis. As we will see, the factor of $\sqrt{5}$ in the denominator of the expression for $m_{B'}$ will have important phenomenological consequences.

The Higgs sector contains a scalar triplet in addition to a SM-like scalar doublet. The doublet and triplet both obtain vevs. The doublet vev, v, brings about electroweak symmetry breaking (EWSB) as in the SM, and thus $v = 246\,\text{GeV}$. The triplet vev, v', is related to v by the couplings in the Coleman-Weinberg potential. Taking these to be $\mathcal{O}(1)$ gives the relation $v' \simeq v^2/2f$.

After EWSB, the mass eigenstates are obtained via mixing between the heavy (W' and B') and light (W and B) gauge bosons. They include the light (SM-like) bosons $W_L^\pm$, Z_L, and A_L observed in experiment, and new heavy bosons $W_H^\pm$, Z_H, and A_H that could be observed in future experiments. At tree level, the processes $e^+e^- \to f\bar{f}$ and $e^+e^- \to Zh$ involve the exchange of only the neutral gauge bosons. Their masses are given by

$$\begin{aligned}
M_{A_L}^2 &= 0, \\
M_{Z_L}^2 &= m_Z^2\left[1 - \frac{v^2}{f^2}\left(\frac{1}{6} + \frac{1}{4}(c^2 - s^2)^2 + \frac{5}{4}(c'^2 - s'^2)^2\right) + 8\frac{v'^2}{v^2}\right], \\
M_{A_H}^2 &= m_Z^2 s_w^2\left(\frac{f^2}{5s'^2c'^2v^2} - 1 + \frac{x_H c_w^2}{4s^2c^2s_w^2}\right), \\
M_{Z_H}^2 &= m_W^2\left(\frac{f^2}{s^2c^2v^2} - 1 - \frac{x_H s_w^2}{4s'^2c'^2c_w^2}\right),
\end{aligned} \tag{6}$$

where m_W and m_Z are the SM gauge boson masses, and s_w (c_w) represents the sine (cosine) of the weak mixing angle. Here x_H, given by [11]

$$x_H = \frac{5}{2}gg'\frac{scs'c'(c^2s'^2 + s^2c'^2)}{5g^2s'^2c'^2 - g'^2s^2c^2}, \tag{7}$$

characterizes the mixing between B' and W'^3 in the A_H and Z_H eigenstates. It is important to note that the first term in the parentheses for $M_{A_H}^2$ and $M_{Z_H}^2$ dominates the rest. As a result, $M_{A_H}^2$ depends strongly on s' and not on s, and vice versa for $M_{Z_H}^2$. This dependence

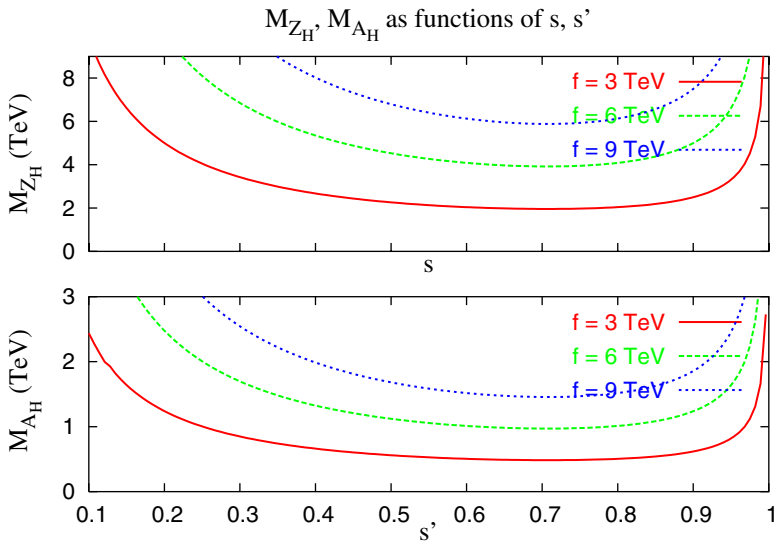

Figure 1: Dependence of the heavy gauge boson masses M_{Z_H} and M_{A_H} on s and s', respectively, for different values of f.

is shown in Fig. 1. Note that the A_H is significantly lighter than the Z_H and can be as light as a few hundred GeV; we will discuss the consequences of this below.

After EWSB, the couplings of the gauge bosons Z_L, A_H, and Z_H to fermions similarly depend on s, s' and f because of the mixing between the fields. If we demand that the U(1) be anomaly-free, which requires $y_u = -2/5$ and $y_e = 3/5$ in the notation of [11], the general structure of the couplings is

$$\begin{aligned} g(A_L f\bar{f}) &= g_{SM}(Af\bar{f}), \\ g(Z_L f\bar{f}) &= g_{SM}(Zf\bar{f})\left(1 + \frac{v^2}{f^2}a_i(s,s')\right), \\ g(A_H f\bar{f}) &= b_i \frac{g'}{2s'c'}(\frac{1}{5} - \frac{1}{2}c'^2), \\ g(Z_H f\bar{f}) &= \pm\frac{gc}{4s}, \end{aligned} \tag{8}$$

where g_{SM} represents the relevant coupling in the SM. A and Z are the SM photon and Z boson, and a_i and b_i are both $\mathcal{O}(1)$ where i labels the species of fermion.

The existence of the heavy gauge boson-Higgs couplings is a hallmark of the Littlest Higgs model. They can be probed using the process $e^+e^- \to Z_L H$ through the exchange of

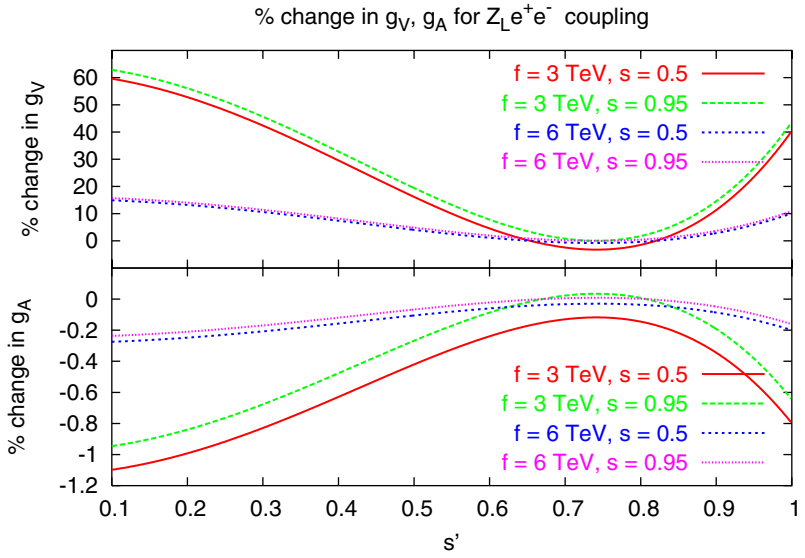

Figure 2: The percent deviation of the vector and axial $Z_L e\bar{e}$ couplings from the SM values for $Z_{SM} e\bar{e}$, taking various values for the parameters f and s.

the Z_L, Z_H, and A_H. The relevant couplings are given by

$$\begin{aligned} g(Z_{L\mu} Z_{L\nu} H) &= g_{SM}(Z_\mu Z_\nu H)\left(1 + \frac{v^2}{f^2} a(s,s')\right), \\ g(Z_{L\mu} Z_{H\nu} H) &= \frac{-i}{2}\frac{g^2}{c_W} v \frac{c^2 - s^2}{2sc} g_{\mu\nu}, \\ g(Z_{L\mu} A_{H\nu} H) &= \frac{-i}{2}\frac{gg'}{c_W} v \frac{c'^2 - s'^2}{2s'c'} g_{\mu\nu}. \end{aligned} \tag{9}$$

where a is an $\mathcal{O}(1)$ function. The formulae for the couplings can be found in Appendix B of the first paper in [11].

Certain bounds on s and s' can be obtained by requiring that these couplings remain perturbative. Using the convention that a perturbative coupling g satisfies $g^2/4\pi < 1$ gives $s, s' \gtrsim 0.1 - 0.2$. Using the more conservative convention $g^2 < 1$ would give a smaller allowed range for the parameters. In the analysis that follows, we include the region where $s > 0.16$. As discussed above, expectations for the value of f arise from the requirement of naturalness. For $f \gtrsim 10\,\text{TeV}$, the LH model no longer addresses the hierarchy problem.

As in [11], we write the fermion-boson coupling as $i\gamma^\mu(g_V + g_A\gamma^5)$. It turns out that for the electron-Z_L coupling, $|g_A| \gg |g_V|$, while in general the shifts in the couplings due to mixing are roughly equal, *i.e* $|\Delta g_A| \simeq |\Delta g_V|$. Thus the relative change in g_V is in general much greater than that for g_A, as shown in Fig. 2. This relative change in g_V is numerically fairly unimportant for most of the observables in our analysis, as the cross sections are typically functions of $g_V^2 + g_A^2$. The left-right asymmetry A_{LR}, however, has terms directly proportional to g_V. Therefore, for the ILC, which has beam polarization capability, the A_{LR}

deviation is important and introduces a surprising s' dependence in our results. We will discuss this in greater detail in Sec. 3.

Equation 6 shows that for generic choices of s and s', $M_{A_H}/M_{Z_H} \simeq s_w m_Z/\sqrt{5}m_W \simeq 1/4$. Figure 1 illustrates this, with M_{A_H} dipping well below 1 TeV for much of the parameter space. As mentioned in Sec. 1, this light A_H is responsible for the most stringent experimental constraints on the model [5, 9]. As a result, phenomenologically viable variations of the Littlest Higgs models typically decouple the A_H by modifying the gauge structure of the theory as in [12] and [13]. In this paper, however, we analyze the original Littlest Higgs model as it is the most phenomenologically well-studied. To gain some understanding of models in which the A_H decouples we take two approaches in our analysis. One is to choose a parameter value ($s' = \sqrt{3/5}$) for which the coupling of A_H to fermions vanishes. This decouples the A_H from all tree-level electron-positron collider physics. Another approach is to artificially take $M_{A_H} \to \infty$ while letting all other quantities in the theory take on their usual, parameter-dependent values. While not theoretically consistent, this approach gives us a more general picture of the behavior of models in which the A_H decouples. We take both approaches and show the results for each case throughout our analysis.

3 Parameter Determination via $e^+e^- \to f\bar{f}$

In this section we examine the process $e^+e^- \to f\bar{f}$, where all of the LH neutral gauge bosons participate via s-channel exchange, at past and future colliders. We first use a χ-square analysis using the $e^+e^- \to f\bar{f}$ observables measured at LEP II. This analysis gives the region of LH parameter space excluded (to 95% confidence level) by the LEP II data.

We then perform a similar χ-square analysis at the energies and luminosity expected at the ILC. We use the same set of observables as in the LEP II analysis as well as the polarization asymmetries that will be measurable due to the beam polarization capability at the ILC. This analysis gives the region of LH parameter space for which the ILC will be able to determine (to 95% confidence level) that the data cannot be explained by the Standard Model, and represents the ILC Littlest Higgs search reach. The two analyses just mentioned are described in Sec. 3.1.

Finally, in Sec. 3.2, we examine the ability of the ILC to determine the values of the LH parameters from $e^+e^- \to f\bar{f}$. For a few different generic sets of LH parameters, we first generate sample data for the observables, and then perform a χ-square analysis to map out the region in LH parameter space that is inconsistent (to 95% CL) with the sample data. The size and shape of the remaining region tells us how accurately LH parameters can be determined.

3.1 The LEP II exclusion region and ILC search reach

Here we present our numerical analysis of the experimental constraints on the Littlest Higgs parameter space from LEP II data as well as the search reach expected from the ILC. We use the Lagrangian and Feynman rules of the Littlest Higgs model as described in [11]. Note that for our analysis, we follow the notation of [11] and take the values of the U(1) charge

parameters $y_u = -2/5$ and $y_e = 3/5$ that, as previously discussed, leave the U(1) anomaly-free and give the couplings shown in Eq. 8. The remaining free parameters of the model that are relevant to $e^+e^- \to f\bar{f}$ are the sines of the two $[SU(2) \times U(1)]$ mixing angles, s and s'; and the "decay constant," or vev, f as defined in Eq. 1 and Eq. 5.

We first study the constraints on the model from $e^+e^- \to f\bar{f}$ at LEP II, taking as our observables the normalized, binned angular distribution and total cross section for $e^+e^- \to b\bar{b}$, $c\bar{c}$, and $l\bar{l}$, with $l = e$, μ, or τ. We use $\sqrt{s} = 200\,\mathrm{GeV}$ and an integrated luminosity $\mathcal{L}$= 627 pb^{-1}. For the detection efficiencies, we take $\epsilon_e = 97\%$, $\epsilon_\mu = 88\%$, $\epsilon_\tau = 49\%$, $\epsilon_b = 40\%$, and $\epsilon_c = 10\%$ [14]. We perform a χ-square analysis and take the SM values for all the observables to correspond to $\chi^2 = 0$, with a nonzero χ^2 representing deviation from the SM. This is a reasonable approach, since there was no detectable deviation from the SM at LEP II [14].

For the ILC analysis, in addition to the above mentioned observables, we also include the angular binned left-right asymmetry A_{LR} for each fermion pair. We use the projected energy $\sqrt{s} = 500$ GeV and luminosity $\mathcal{L}$= 500 fb^{-1}. For the detection efficiencies, we take $\epsilon_e = 97\%$, $\epsilon_{\mu,\tau} = 95\%$, $\epsilon_b = 60\%$, and $\epsilon_c = 35\%$ [15].

Because of the presence of the Z_H and A_H, we use a general formula for the differential cross section for $e^+e^- \to f\bar{f}$ that is valid for any set of extra gauge bosons that can run in the s-channel [16],

$$\frac{d\sigma}{dz} = C_\mathrm{f}\frac{s}{32\pi}\sum_{ij} P_{ij}^{ss}[B_{ij}(1+z^2) + 2C_{ij}z], \tag{10}$$

where $z \equiv \cos\theta$, C_f is the color factor,

$$P_{ij}^{ss} \equiv \frac{(s-M_i^2)(s-M_j^2) + (\Gamma_i M_i)(\Gamma_j M_j)}{[(s-M_i^2)^2 + (\Gamma_i M_i)^2][(s-M_j^2)^2 + (\Gamma_j M_j)^2]}, \tag{11}$$

and

$$B_{ij} \equiv (v_i v_j + a_i a_j)_f (v_i v_j + a_i a_j)_e\,,\ C_{ij} \equiv (v_i a_j + a_i v_j)_f (v_i a_j + a_i v_j)_e.$$

Here v and a correspond to the vector and axial couplings g_V and g_A discussed in Sec. 2, and the sum runs over the gauge bosons in the s-channel: A_L, Z_L, A_H, and Z_H.

For Bhabha scattering, besides the s-channel, we also have a contribution from the t-channel, so that

$$\begin{aligned}\frac{d\sigma}{dz} = \frac{s}{32\pi}\sum_{ij}\Bigg\{ & P_{ij}^{ss}\left[B_{ij}(1+z^2) + 2C_{ij}z\right] + \\ & 2P_{ij}^{tt}\left[B_{ij}\left(1+\frac{1}{4}(1+z)^2\right) - C_{ij}\left(1-\frac{1}{4}(1+z)^2\right)\right] + \\ & P_{ij}^{st}(1+z)^2(B_{ij}+C_{ij})\Bigg\},\end{aligned} \tag{12}$$

where P_{ij}^{st} and P_{ij}^{tt} are defined similarly to P_{ij}^{ss} with the replacement $s \to t = -\frac{1}{2}s(1-z)$ in Eq. 11 in the obvious way.

To calculate A_{LR}, we need the cross sections for left- and right-handed electrons. These can be obtained from the above formulae by making the replacements

$$v_{ie} \to \frac{1}{2}\left(v_{ie} + \lambda a_{ie}\right),\ a_{ie} \to \frac{1}{2}\left(a_{ie} + \lambda v_{ie}\right), \tag{13}$$

with $\lambda = +1(-1)$ corresponding to left- (right-) handed electrons. Then the left-right asymmetry is given by

$$A_{LR}(z) = \mathcal{P}\frac{\frac{d\sigma_L}{dz} - \frac{d\sigma_R}{dz}}{\frac{d\sigma_L}{dz} + \frac{d\sigma_R}{dz}}, \tag{14}$$

where $\mathcal{P}$ is the degree of e^- beam polarization at the ILC, which we take to be 80%. We assume the e^+ beam is unpolarized.

We compute the χ^2 distribution as follows, where σ^i represents one of the observables mentioned above:

$$\chi^2 = \sum_i \left(\frac{\sigma^i_{LH} - \sigma^i_{SM}}{\delta\sigma^i}\right)^2. \tag{15}$$

Here, $\delta\sigma$ is the statistical error for each observable, given by

$$\begin{aligned}
\delta\sigma_{tot} &= \sqrt{\frac{\sigma_{tot}}{\mathcal{L}\epsilon}}, \\
\delta(\frac{d\sigma_N}{dz}) &= \sqrt{\frac{\frac{d\sigma_N}{dz} - (\frac{d\sigma_N}{dz})^2}{\mathcal{L}\epsilon\sigma_{tot}}}, \\
\delta A_{LR} &= \sqrt{\frac{1 - A^2_{LR}}{\mathcal{L}\epsilon\sigma_{tot}}},
\end{aligned} \tag{16}$$

where σ_{tot} is the total cross section and $\frac{d\sigma_N}{dz}$ is the normalized differential cross section. The efficiency ϵ for each final state is given above.

As previously noted, s, s', f are the free parameters present in the neutral gauge sector of the LH model. In our analysis, we choose a fixed value of s' and scan the parameter space (s, f).

The exclusion region at LEP II and the search reach at the ILC correspond to the regions where χ^2 is greater than 5.99, representing a 95% confidence level for two free parameters. The combined result is shown in Fig. 3 for different values of s'. For each value of s', the LEP II exclusion region and the ILC search reach are on the left of the corresponding contour. This is because as f increases, the gauge boson masses (proportional to f) also increase (see Fig. 1) and the deviations in the $Z_L f\bar{f}$ couplings (proportional to v^2/f^2) decrease. For the ILC search reach boundary one would expect to see four contours at the upper right corner corresponding to the four different input values of s'. However, there is only one visible contour, for $s' = \sqrt{3/5}$, because in the other three cases, the search reach covers the entire parameter space shown in the figure.

As discussed above, the choice $s' = \sqrt{3/5}$ corresponds to decoupling the A_H from the fermion sector, as verified by the results shown in Eq. 8. In this case, the ILC search reach

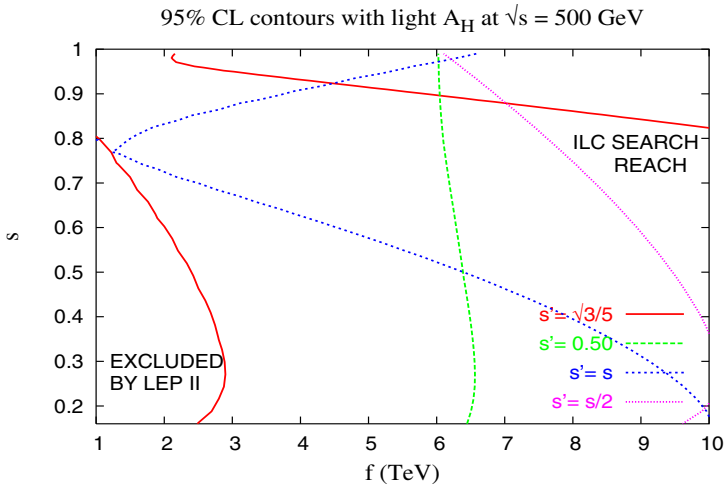

Figure 3: LEP II exclusion region from $e^+e^- \to f\bar{f}$ and ILC search reach in the parameter space (s, f) for different input values of s', and including the A_H contribution. For $s' = \sqrt{3/5}$ there are two lines of the same symbol/color, one on the boundary of the LEP II exclusion region, and one on the boundary of the ILC search reach region. For the other values of s' the curve shown is the boundary of the LEP II exclusion region, while the ILC search reach covers the entire parameter region shown.

can be as low as $f \sim 2\,\text{TeV}$ for large values of s. For other values of s', the search reach is greater than $f \sim 10\,\text{TeV}$ for all values of s. We thus see how strongly the presence of the relatively-light A_H can affect the phenomenology. For LEP II, the story is similar; the exclusion region for $s' = \sqrt{3/5}$ is much smaller than for other values of s'. This is because the observed deviation at $s' = \sqrt{3/5}$ is solely due to the modification in the $Z_L f\bar{f}$ coupling and the presence of the Z_H, which is generally several times heavier than the A_H. For other values of s' the constraints on f can be as high as ~ 6 TeV. Overall, the LEP II exclusion regions have constraints on the parameter f that are roughly consistent with those from precision measurements [1, 5, 6, 7, 8, 9].

As discussed in Sec. 2, we also examine the general behavior of models in which the A_H is decoupled by taking $M_{A_H} \to \infty$ while letting all other quantities take on their usual values. The results in this case are presented in Fig. 4. It is not surprising that the $s' = \sqrt{3/5}$ contours in Fig. 4 are exactly the same as in Fig. 3, since the A_H is decoupled for this choice of s'. For other values of s', the contours are very different in the two cases. The s dependence of the contours in Fig. 4 is easy to understand. The $Z_H f\bar{f}$ couplings go as gc/s, thus the ILC contours show that the search reach is higher for lower values of s. Similarly, for LEP II, the exclusion region extends farther out in f for lower values of s. There is, however, a "turnover" for the LEP II exclusion region around $s \sim 0.3$ where the contours start moving towards lower f. This takes place because the mass M_{Z_H} begins to increase (see Fig. 1) and the overall contribution from Z_H to the observables starts to decrease as s gets smaller.

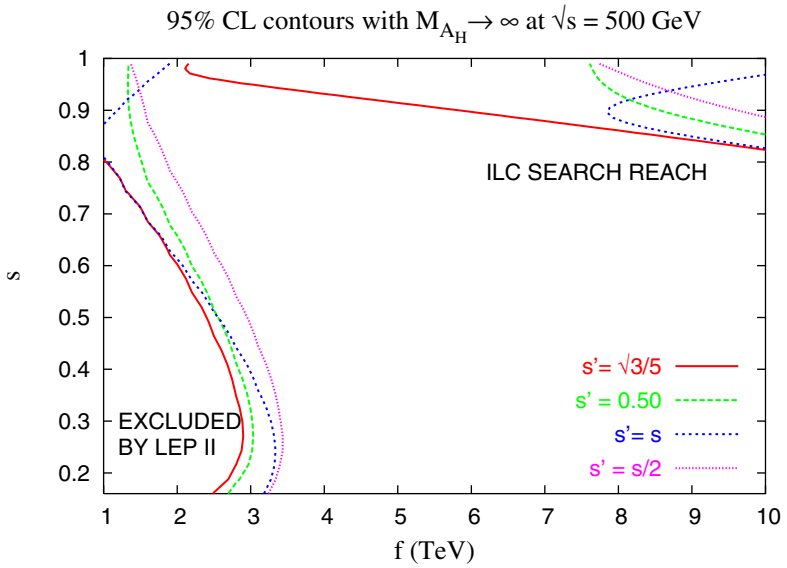

Figure 4: LEP II exclusion region and ILC search reach as in Fig. 3, but with $M_{A_H} \to \infty$.

With $M_{A_H} \to \infty$, the s'-dependence of the χ^2 is mostly due to the deviation in the $Z_L f\bar{f}$ couplings, since neither the $Z_H f\bar{f}$ couplings (see Eq. 8) nor M_{Z_H} (see Eq. 6) are strongly dependent on s'. This explains why there is less variation among the different contours in Fig. 4 than in Fig. 3. For values of s close to 1, however, the ILC contours for different values of s' begin to deviate from one another markedly. This s' dependence is due to the s'-sensitive deviation of A_{LR}, as discussed in Sec. 2. This is confirmed by Fig. 5, which shows the relative contribution of the different observables to the χ^2 at the ILC with $M_{A_H} \to \infty$ and $s = 0.95$. Note that A_{LR} for various final states dominates the χ^2 where it is large.

The fact that the search reach is lowest for $s' = \sqrt{3/5}$ then indicates that the deviations in the $Z_L f\bar{f}$ couplings are smallest for this parameter value. This coincidence arises because both A_H and Z_L are linear combinations of gauge eigenstates. A_H to lowest order is just B', whose couplings to fermions vanish at $s' = \sqrt{3/5}$. As the s'-dependent terms in the deviation of the $Z_L f\bar{f}$ couplings arise from the B' admixture, they also vanish at this value. This is also confirmed by Fig. 5, which shows that the relative contribution of A_{LR} and the total χ^2 decrease around $s' = \sqrt{3/5}$.

The search reach at a $\sqrt{s} = 1\,\text{TeV}$ ILC reaches to somewhat higher values of the parameter s, but has essentially the same reach for the parameter f as the $\sqrt{s} = 500\,\text{GeV}$ machine. This is reasonable; as s approaches unity, the contribution from the deviations in the Z_L couplings dominates the search reach, and these contributions are not as important as the center of mass energy increases. The result is that the search reach is very simlar for both $\sqrt{s} = 500$ GeV and 1 TeV. We will see later, however, that the $\sqrt{s} = 1\,\text{TeV}$ data can significantly improve the parameter determination.

Figure 3 and Fig. 4 show that the $\sqrt{s} = 500\,\text{GeV}$ ILC search reach in general covers most of the interesting parameter space where the Littlest Higgs models are relevant to the

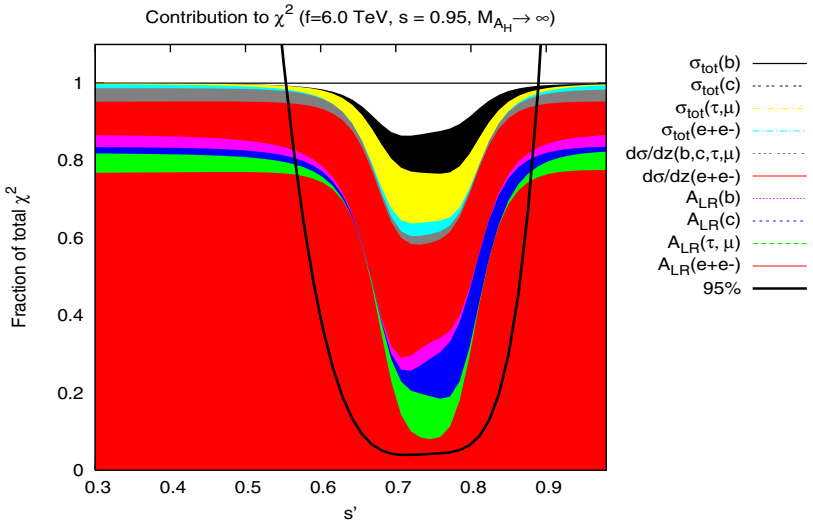

Figure 5: Fractional contribution to the total χ^2 for each $e^+e^- \to f\bar{f}$ observable at a 500 GeV ILC for fixed (s, f). The labels on the legend go from top down in one-to-one correspondence with the shaded sections. For example, $A_{LR}(e^+e^-)$ contributes $\sim 78\%$ to the total χ^2 at $s' = 0.4$. The line labeled "95%" is the total $\chi^2/5.99$. This means that the region $s' \sim [0.55, 0.9]$ where this line dips below 1 is outside the $\sqrt{s} = 500$ GeV ILC search reach.

gauge hierarchy. Thus the $e^+e^- \to f\bar{f}$ process alone is an effective tool for investigating the Littlest Higgs model at a ILC.

3.2 Parameter Determination: sample fits

We have now determined the available parameter space accessible to the ILC and not already excluded by LEP II. It remains to ask, given the existence of an LH model with parameters in this accessible range, how accurately would the ILC be able to measure them? To answer this question we perform some sample fits, using a χ-square analysis similar to the one described in the preceding section. We use the same ILC observables as before. In some cases we also include data from a $\sqrt{s} = 1$ TeV run, for which we also take an integrated luminosity of $\mathcal{L}$= 500 fb^{-1}. We note that we can exchange M_{Z_H} for f, so we now take M_{Z_H}, s, and s' as our free parameters. We choose a generic data point (s, s', M_{Z_H}) and use it to calculate the observables, which we then fluctuate according to statistical error. We assume that the Large Hadron Collider would have determined M_{Z_H} relatively well, to the order of a few percent for $M_{Z_H} \lesssim 5 - 6$ TeV; we thus fix M_{Z_H} and perform a 2-variable fit to s and s'. Scanning the s-s' parameter space, we calculate the χ^2 at every point. We find the minimum χ^2 point; the 95% CL region surrounding it is the region for which the χ^2 is less than this minimum χ^2 plus 5.99.

Figure 6 shows the results of this fit for two sample data points in the contrived scenario with $M_{A_H} \to \infty$. For both of these points, the determination of s is very accurate. This

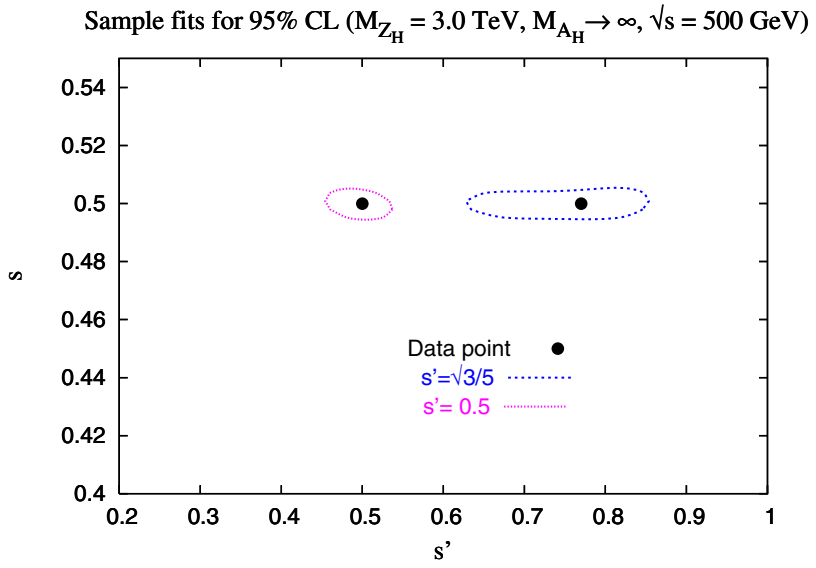

Figure 6: 95% CL sample fits to the data points ($s = 0.5$, $s' = 0.5$) and ($s = 0.5$, $s' = \sqrt{3/5}$), using $e^+e^- \to f\bar{f}$ observables at a 500 GeV ILC, taking $M_{Z_H} = 3.0\,\text{TeV}$ and $M_{A_H} \to \infty$.

is due to the strong dependence of the $Z_H f\bar{f}$ couplings on s, as discussed in the previous section. The s' determination is worse than that for s because of our choice $s = 0.5$. At this value of s, the contributions from the Z_L coupling deviations (which carry the s' dependence) are smaller than the Z_H contributions. The reason the s' determination is better for $s' = 0.5$ than it is for $s' = \sqrt{3/5}$ is that the s'-dependent deviations in $g_{V_{Z_L f\bar{f}}}$ vanish for the latter value.

Figure 7 shows the results from a similar fit and illustrates how it can be improved with data from a higher-energy run with $\sqrt{s} = 1\,\text{TeV}$ at the ILC. Here, the s determination is not much more accurate than the s' determination, as the s'-independent Z_H contributions no longer dominate the fit for $s = 0.9$.

In Fig. 8 we show results from a fit with the full A_H contributions. Not surprisingly, the parameter determination is much more precise, as the A_H contributions, when present, dominate the χ^2. Since the A_H couplings depend only on s', it is also no surprise that here the s' determination is in general much better than that for s.

If, for some reason, the LHC doesn't provide a good measurement of M_{Z_H}, we would need to include that quantity, or equivalently f, in our fits to the data. In Fig. 9 we show the results where we have set $s' = \sqrt{3/5}$ and we fit to s and f. Note that for one of the data points, the allowed region doesn't close. This highlights the importance of using both the LHC and the ILC to reliably determine the model parameters.

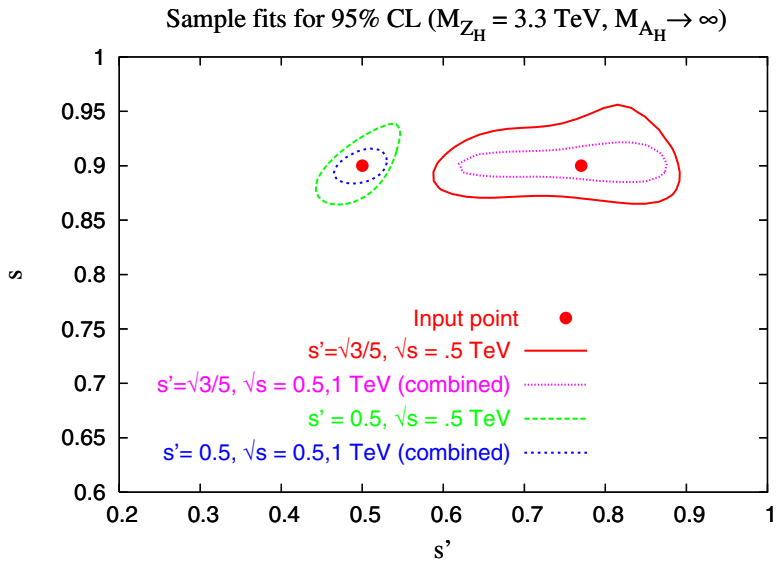

Figure 7: Like Fig. 6 except $M_{Z_H} = 3.3\,\text{TeV}$ and the data points are ($s = 0.9$, $s' = 0.5$) and ($s = 0.9$, $s' = \sqrt{3/5}$). Also shown for each point is an improved fit from adding data from a $\sqrt{s} = 1\,\text{TeV}$, $\mathcal{L}$= 500 fb^{-1}run at the ILC.

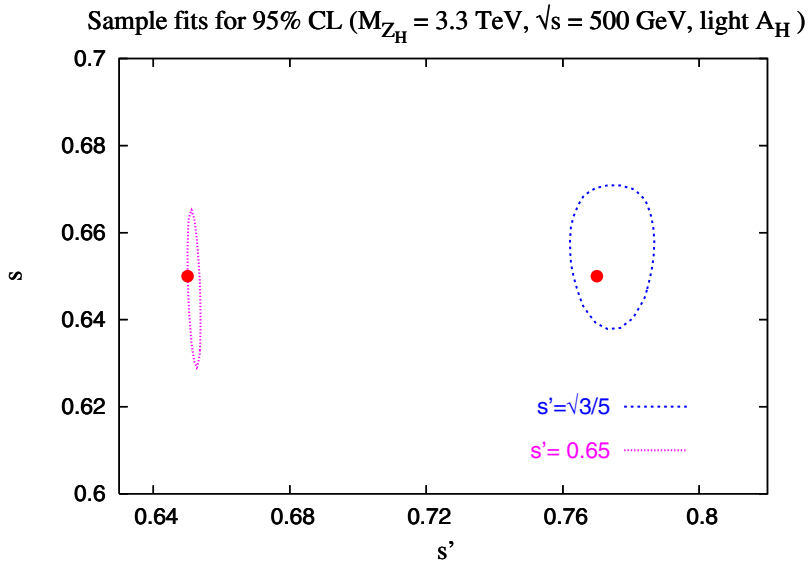

Figure 8: Like Fig. 6, except $M_{Z_H} = 3.3\,\text{TeV}$ and the data points are ($s = 0.65$, $s' = 0.65$) and ($s = 0.65$, $s' = \sqrt{3/5}$), and the full M_{A_H} contributions are included.

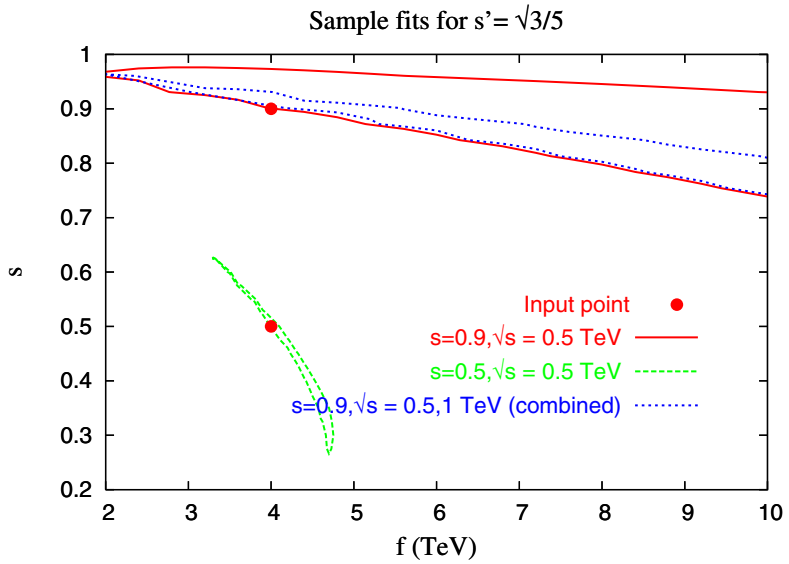

Figure 9: Sample fits to the data points ($s = 0.5$, $f = 4\,\text{TeV}$) and ($s = 0.9$, $f = 4\,\text{TeV}$), taking $s' = \sqrt{3/5}$. At the decoupling value of s', the A_H does not contribute.

4 Parameter determination using $e^+e^- \to Z_L h$

In order to confirm that the LH model is the correct description of TeV-scale physics, it is important to test the hallmark of the LH mechanism, namely that the Higgs mass quadratic divergences are canceled by new particles with the same spin as their SM counterparts. The proof lies in the measurement of the new particle couplings to the Higgs. Here we are concerned with the coupling of the heavy Z to the Higgs boson. This coupling can be tested via the process $e^+e^- \to Z_L h$. In the LH model, deviations of observables related to this process from their SM expectations come from three sources: the diagram with the Z_H in the s-channel, the diagram with the A_H in the s-channel, and the deviation of the $Z_L Z_L h$ coupling from its SM value.

In this section we repeat the analysis of Section 3, using the process $e^+e^- \to Z_L h$ and taking the total cross section as our observable with $m_h = 120\,\text{GeV}$. We assume that at a $\sqrt{s} = 500\,\text{GeV}$ ILC this cross section will be measured to an accuracy of 1.5% [15].

The cross section, including the effects of additional gauge bosons, can be written as

$$\sigma_{Z_L h} = \frac{|\mathbf{k}|}{8\pi\sqrt{s}}\left(1 + \frac{|\mathbf{k}|^2}{3m_Z^2}\right)\sum_{ij} P_{ij}^{ss}[g_{iZ_Lh}g_{jZ_Lh}(v_i v_j + a_i a_j)_e], \tag{17}$$

where P_{ij}^{ss} was defined in Eq. 11. The sum runs over the participating gauge bosons in the s-channel: Z_L, A_H, and Z_H. Here, $|\mathbf{k}|$ is the magnitude of the 3-momentum of the outgoing Z_L, given by

$$|\mathbf{k}| = \frac{1}{2\sqrt{s}}\sqrt{(m_H^2 - M_{Z_L}^2)^2 + s(s - 2(M_{Z_L}^2 + m_H^2))}. \tag{18}$$

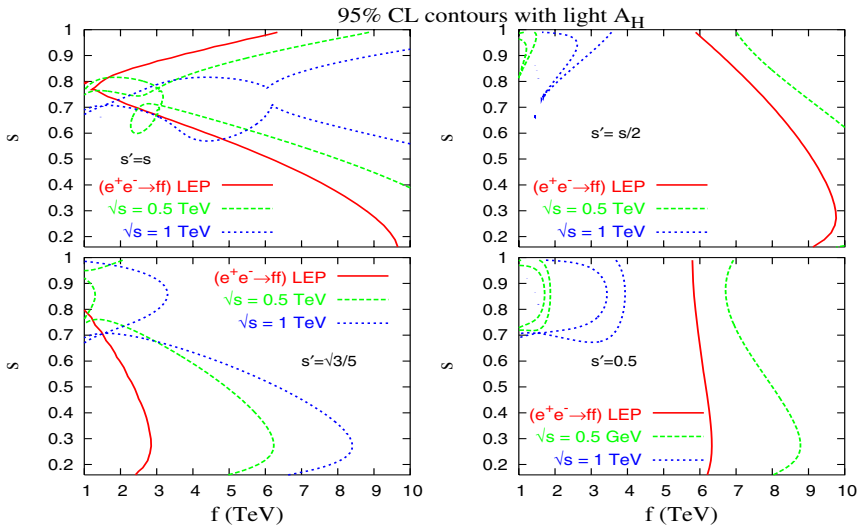

Figure 10: LEP II exclusion region from $e^+e^- \to f\bar{f}$ and ILC search reach in the parameter space (s, f) from the process $e^+e^- \to Z_L h$, for various values of s' and including the full A_H contributions. For each value of s' there are three curves; one corresponds to the LEP II exclusion region, and the other two represent the ILC search reach region for $\sqrt{s} = 500$ and 1000 GeV, respectively, taking an integrated luminosity of 500 fb^{-1}at each center-of-mass energy.

The couplings v_i and a_i are the same as before–the axial and vector couplings of electrons to the ith gauge boson.

We carry out the χ-square analysis as before. Figure 10 shows the ILC search reach in the LH parameter space, where each plot corresponds to a different choice of s'. By comparing to Fig. 4 we note that $e^+e^- \to Z_L h$ gives a much poorer search reach than $e^+e^- \to f\bar{f}$. In particular, when s' is near the decoupling value $\sqrt{3/5}$ the LH model is generally indistinguishable from the SM. Well away from $s' = \sqrt{3/5}$, as shown for $s' = s/2$ and $s' = 0.5$, the search reach covers almost all of parameter space, except for regions of low f where interference between the A_H and Z_H conspire to bring the cross section near its SM value. These regions, however, are ruled out by LEP.

In the case $s' = s$, however, there are regions that exhibit similar interference effects and are not ruled out by LEP data. For example, consider the two data points $f = 4.0$ TeV, $s = 0.61$ with (a) $s' = \sqrt{3/5}$ and (b) $s' = 0.61$. With $\sqrt{s} = 500$ GeV, (b) is within the search reach while (a) is just outside the search reach. Figure 11 shows that at this value of $\sqrt{s}$, the deviation of the cross section from the SM is much greater for $s' = 0.61$ than for $s' = \sqrt{3/5}$, since the A_H decouples in the latter case. With $\sqrt{s} = 1$ TeV, this behavior is reversed; point (a) is outside the search reach while (b) is within. At this value of $\sqrt{s}$ the interference between A_H and Z_H brings the cross section closer to the SM value when the A_H contributes.

Figure 12 shows the search reach obtainable with 500 fb^{-1}at a $\sqrt{s} = 500$ GeV ILC, taking

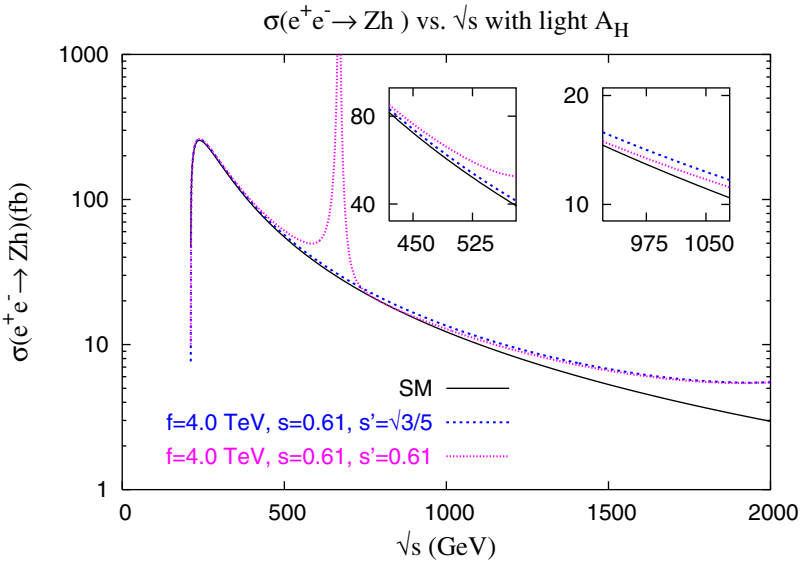

Figure 11: The cross section for $e^+e^- \to Z_L h$ as a function of $\sqrt{s}$ for the SM and two different points in LH parameter space. The insets show the behavior near the expected ILC $\sqrt{s}$ values of 500 GeV and 1 TeV. The resonance at about 700 GeV corresponds to the A_H.

$M_{A_H} \to \infty$. Comparing to Fig. 3, we see that the search reach here is much smaller than for $e^+e^- \to f\bar{f}$. Figure 13 displays the corresponding reach at $\sqrt{s} = 1\,\text{TeV}$ with 500 fb^{-1}. In both cases, and for all choices of s', the search reach decreases markedly around $s = \sqrt{2}$. This is because the $Z_L Z_H H$ coupling vanishes at this value of s, as can be seen in Eq. 9. It is also interesting to note that the spread in the search reach as s' is varied is larger for $\sqrt{s} = 500\,\text{GeV}$ than it is for 1 TeV. This can be understood if one notes that $\sqrt{s} = 1\,\text{TeV}$ is closer to the Z_H pole (as $M_{Z_H} \simeq$ a few TeV throughout the parameter space) than is 500 GeV. Thus the deviation of σ_{Zh} from its SM value at $\sqrt{s} = 1\,\text{TeV}$ is dominated by the presence of the Z_H, whose mass and couplings are essentially s'-independent. At $\sqrt{s} = 500\,\text{GeV}$, the deviation of σ_{Zh} has a more significant contribution from the deviation of the $e^+e^-Z_L$ coupling, which is strongly dependent on s' (see Fig. 2). For both values of $\sqrt{s}$, the sensitivity in the range of parameter space where $s \gtrsim 0.5$ does not reach beyond the general precision electroweak bound of $f \gtrsim 4\,\text{TeV}$.

One could hope to improve the sensitivity by adding the measurement of the Higgs branching ratios as additional observables. It turns out, however, that the LH deviations of the branching ratios from their SM values are at most 1-2%, which is smaller than or equivalent to the experimental sensitivity at the ILC.

5 Summary

Little Higgs models provide an interesting mechanism for addressing the hierarchy problem. They contain a single light Higgs boson which is a pseudo-Goldstone boson with a small

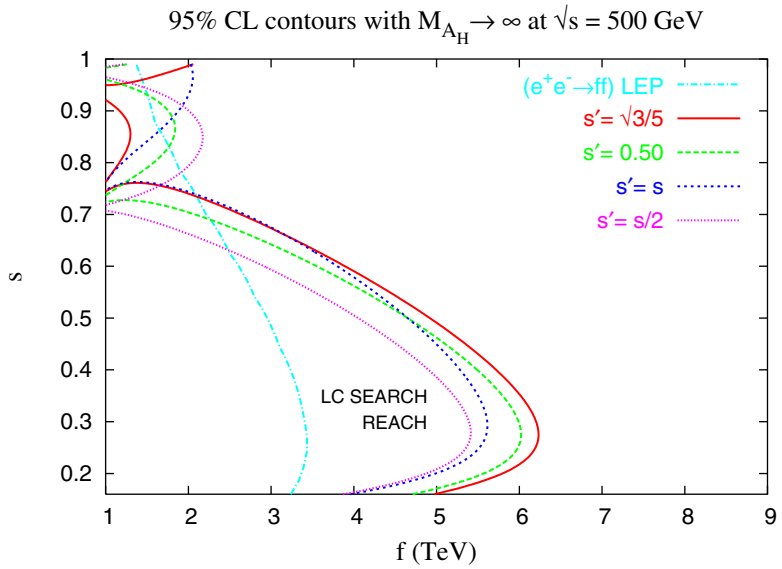

Figure 12: The ILC search reach from the process $e^+e^- \to Z_L h$ for various values of s', taking $\sqrt{s} = 500$ and $M_{A_H} \to \infty$. The LEP II exclusion region from $e^+e^- \to f\bar{f}$ is shown for $s' = s/2$ (from Fig. 4) for comparison.

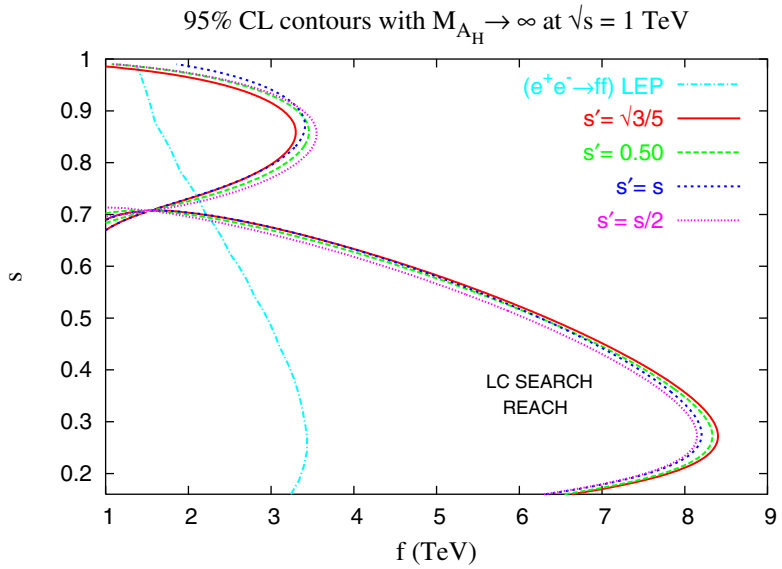

Figure 13: Same as Fig. 12, but for $\sqrt{s} = 1\,\text{TeV}$.

mass generated at the two-loop level. The quadratically divergent loop contributions to the mass of this Higgs are canceled by contributions from new particles appearing at the TeV scale. These cancelations take place between contributions from particles which have the same spin. Measurement of the couplings of these new particles to the light Higgs would verify the structure of these cancelations and establish the Little Higgs mechanism.

Here, we have investigated the extended gauge boson sector within these theories. Numerous Little Higgs models, based on various global symmetries, have been proposed. However, the existence of an enlarged gauge sector, with rather generic features, is endemic to all these scenarios. We choose to work in the framework of the simplest model of this type, known as the Littlest Higgs, based on an SU(5)/SO(5) nonlinear sigma model. This scenario contains the new heavy gauge bosons $W_H^{\pm}$, Z_H, and A_H in addition to the SM gauge fields. The masses of these additional gauge bosons are expected to be of order the global symmetry breaking scale of $f \sim$ TeV. (It is expected that $f \lesssim 10$ TeV in order for this scenario to be relevant to the hierarchy.) However, due to the group theory structure, the A_H can be significantly lighter resulting in stringent constraints from precision electroweak data. Phenomenologically viable Littlest Higgs models must thus decouple the A_H and we have examined two such approaches in our analysis. One, where we choose the model parameters such that the fermion couplings of the A_H vanish, and another where we artificially take $M_{A_H} \to \infty$.

We study the effects of the new neutral gauge bosons in e^+e^- annihilation. These particles can participate in $e^+e^- \to f\bar{f}$ and $e^+e^- \to Zh$ via s-channel exchange, and their effects can be felt indirectly for center of mass energies well below their masses. We find that fermion pair production is more sensitive to Little Higgs effects than Zh associated production. We perform a thorough investigation of the model parameter space and find that observables at LEP II exclude the region $f \lesssim 1-3$ TeV, which is consistent with the constraints obtained from precision electroweak data. The search reach of the proposed International Linear Collider, operating at $\sqrt{s} = 500$ GeV, covers essentially the entire parameter region where this model is relevant to the hierarchy, *i.e.*, $f \lesssim 6-10$ TeV. In the case of a 1 TeV ILC, the search region probes slightly larger values of the mixing parameter s, but similar values of f.'

We have also demonstrated that once a signal is observed in these channels, accurate measurements of the couplings of the heavy gauge fields can be obtained from fermion pair production at the ILC. These couplings are related to the mixing angles in the extended gauge sector and we show that experiments at the ILC can determine the fundamental parameters of the theory. For illustration, we performed a fit to generated data for sample points in the Littlest Higgs parameter space, and found that the fundamental parameters can be determined to the precision of a few percent, provided that the LHC measures the mass of the heavy neutral gauge field. If information on the new boson masses is not available from the LHC, then the parameter determination at the ILC deteriorates. Additionally, the couplings of the extra gauge bosons to the light Higgs can separately be determined from $e^+e^- \to Zh$ for a significant region of the parameter space. This enables ILC experiments to test the consistency of the theory and verify the structure of the Higgs quadratic divergence cancelations.

In summary, we find that the ILC has the capability to discover the effects of the Littlest Higgs model over the entire theoretically interesting range of parameters, and to additionally determine the couplings of the heavy gauge bosons to the precision of a few percent.

Acknowledgments

We would like to thank T. Barklow, B. Lillie, H. Logan, M. Peskin, and T. Rizzo for helpful discussions.

References

[1] N. Arkani-Hamed, A. G. Cohen, E. Katz and A. E. Nelson, JHEP **0207**, 034 (2002) [arXiv:hep-ph/0206021].

[2] N. Arkani-Hamed, A. G. Cohen and H. Georgi, Phys. Lett. B **513**, 232 (2001) [arXiv:hep-ph/0105239]; N. Arkani-Hamed, A. G. Cohen, E. Katz, A. E. Nelson, T. Gregoire and J. G. Wacker, JHEP **0208**, 021 (2002) [arXiv:hep-ph/0206020]; I. Low, W. Skiba and D. Smith, Phys. Rev. D **66**, 072001 (2002) [arXiv:hep-ph/0207243]; D. E. Kaplan and M. Schmaltz, JHEP **0310**, 039 (2003) [arXiv:hep-ph/0302049]; S. Chang and J. G. Wacker, Phys. Rev. D **69**, 035002 (2004) [arXiv:hep-ph/0303001].

[3] W. Skiba and J. Terning, Phys. Rev. D **68**, 075001 (2003) [arXiv:hep-ph/0305302]; S. Chang, JHEP **0312**, 057 (2003) [arXiv:hep-ph/0306034].

[4] E. Katz, J. y. Lee, A. E. Nelson and D. G. E. Walker, arXiv:hep-ph/0312287; D. E. Kaplan, M. Schmaltz and W. Skiba, Phys. Rev. D **70**, 075009 (2004).

[5] J. L. Hewett, F. J. Petriello and T. G. Rizzo, JHEP **0310**, 062 (2003) [arXiv:hep-ph/0211218].

[6] M. C. Chen and S. Dawson, Phys. Rev. D **70**, 015003 (2004) [arXiv:hep-ph/0311032].

[7] W. j. Huo and S. h. Zhu, Phys. Rev. D **68**, 097301 (2003) [arXiv:hep-ph/0306029]; C. x. Yue and W. Wang, Nucl. Phys. B **683**, 48 (2004) [arXiv:hep-ph/0401214].

[8] C. Csaki, J. Hubisz, G. D. Kribs, P. Meade and J. Terning, Phys. Rev. D **68**, 035009 (2003) [arXiv:hep-ph/0303236].

[9] C. Csaki, J. Hubisz, G. D. Kribs, P. Meade and J. Terning, Phys. Rev. D **67**, 115002 (2003) [arXiv:hep-ph/0211124].

[10] E. Ros, Eur. Phys. J. C **33**, S732 (2004); C. x. Yue, W. Wang and F. Zhang, arXiv:hep-ph/0409066; G. C. Cho and A. Omote, Phys. Rev. D **70**, 057701 (2004) [arXiv:hep-ph/0408099]; S. C. Park and J. Song, Phys. Rev. D **69**, 115010 (2004); J. J. Liu, W. G. Ma, G. Li, R. Y. Zhang and H. S. Hou, Phys. Rev. D **70**, 015001 (2004) [arXiv:hep-ph/0404171]; G. Azuelos *et al.*, arXiv:hep-ph/0402037; C. x. Yue, S. z. Wang

and D. q. Yu, Phys. Rev. D **68**, 115004 (2003) [arXiv:hep-ph/0309113]; Z. Sullivan, arXiv:hep-ph/0306266; G. Burdman, M. Perelstein and A. Pierce, Phys. Rev. Lett. **90**, 241802 (2003) [Erratum-ibid. **92**, 049903 (2004)] [arXiv:hep-ph/0212228].

[11] T. Han, H. E. Logan, B. McElrath and L. T. Wang, Phys. Rev. D **67**, 095004 (2003) [arXiv:hep-ph/0301040]; T. Han, H. E. Logan and L. Wang, arXiv:hep-ph/0506313.

[12] T. Gregoire, D. R. Smith and J. G. Wacker, Phys. Rev. D **69**, 115008 (2004) [arXiv:hep-ph/0305275].

[13] C. Kilic and R. Mahbubani, JHEP **0407**, 013 (2004) [arXiv:hep-ph/0312053].

[14] G. Abbiendi *et al.* [OPAL Collaboration], Eur. Phys. J. C **33**, 173 (2004) [arXiv:hep-ex/0309053].

[15] J. A. Aguilar-Saavedra *et al.* "Tesla Technical Design Report," arXiv:hep-ph/0106315.

[16] J. L. Hewett and T. G. Rizzo, Phys. Rept. **183**, 193 (1989).